Nonequilibrium dynamics of a singlet–triplet Anderson impurity near the quantum phase transition

2010 J. Phys.: Condens. Matter 22 025602

(http://iopscience.iop.org/0953-8984/22/2/025602)

J. Phys.: Condens. Matter **22** (2010) 025602 (14pp) doi:10.1088/0953-8984/22/2/025602

Nonequilibrium dynamics of a singlet–triplet Anderson impurity near the quantum phase transition

P Roura Bas[1] **and A A Aligia**[2]

[1] Centro Atómico Constituyentes, Comisión Nacional de Energía Atómica, 1650 San Martín, Buenos Aires, Argentina
[2] Centro Atómico Bariloche and Instituto Balseiro, Comisión Nacional de Energía Atómica, 8400 Bariloche, Argentina

E-mail: roura@tandar.cnea.gov.ar

Received 8 August 2009, in final form 16 November 2009
Published 9 December 2009
Online at stacks.iop.org/JPhysCM/22/025602

Abstract
We study the singlet–triplet Anderson model (STAM) in which a configuration with a doublet is hybridized with another containing a singlet and a triplet, as a minimal model to describe two-level quantum dots coupled to two metallic leads in effectively a one-channel fashion. The model has a quantum phase transition which separates regions of a doublet and a singlet ground state. The limits of integer valence of the STAM (which include a model similar to the underscreened spin-1 Kondo model) are derived and used to predict the behavior of the conductance through the system on both sides of the transition, where it jumps abruptly. At a special quantum critical line, the STAM can be mapped to an infinite-U ordinary Anderson model (OAM) plus a free spin 1/2. We use this mapping to obtain the spectral densities of the STAM as a function of those of the OAM at the transition. Using the non-crossing approximation (NCA), we calculate the spectral densities and conductance through the system as a function of temperature and bias voltage, and determine the changes that take place at the quantum phase transition. The separation of the spectral density into a singlet and a triplet part allows us to shed light on the underlying physics and to explain a shoulder observed recently in the zero bias conductance as a function of temperature in transport measurements through a single fullerene molecule (Roch *et al* 2008 *Nature* **453** 633). The structure with three peaks observed in nonequilibrium transport in these experiments is also explained.

(Some figures in this article are in colour only in the electronic version)

1. Introduction

For nearly four decades, the Anderson model for magnetic impurities has been the subject of intense study in condensed matter physics. Its extension to the lattice (or even the impurity model above the so-called coherence temperature) describes, among others, intermediate valence systems [1, 2] and heavy fermions [3, 4]. A bosonic version of it has been used to describe semiconductor microcavities with strong light–matter interaction [5, 6]. The Kondo model is derived through a canonical transformation as an integer valence limit of the Anderson model [7]. The Kondo effect is also one of the most relevant subjects in many-body theory [4]. A strong resurgence of interest in these many-body phenomena has taken place in recent years with experimental results in nanoscale systems. Progress in nanotechnology has made it possible to construct nanodevices in which the Kondo physics is clearly displayed, for example in systems with one quantum dot (QD) [8–10], which constitute ideal systems with a single magnetic impurity in which several parameters can be tuned. Scanning tunneling spectroscopy has made it possible to probe the local density of states near a single impurity and Fano antiresonances have been observed for several magnetic impurities on metal surfaces [11–14]. These antiresonances observed in the differential conductance, are a consequence of a dip in the spectral density of conduction

states caused by the Kondo effect [15–17]. Furthermore, corrals built on the (111) surface of noble metals or Cu have been used to project the spectral features of the Fano–Kondo antiresonance to remote places [11, 17]. The observed Fano lineshapes for one magnetic impurity on these surfaces have been reproduced by many-body calculations [15–21]. The essential physics involved in these nanoscopic systems is well understood in terms of the ordinary Anderson model (OAM). In the following, we denote by OAM the simplest version of the model, with infinite on-site Coulomb repulsion U, in which a configuration with a doublet is hybridized with a singlet. In particular, for systems with one QD with an odd number of electrons, the conductance at zero bias is increased below a characteristic Kondo temperature T_K as a consequence of the Kondo effect. This is a usual feature of single-electron transistors built with semiconductor QDs [8–10] or single molecules [22].

In a QD with an even number of electrons, in many cases, the ground state is a singlet with all dot levels either doubly occupied with both spin projections or empty. In this case, as a gate voltage of either sign is applied, the system goes to a configuration with an odd number of electrons and a doublet ground state. Therefore, the OAM still describes the system at intermediate and even electronic occupation. However, in other cases with an even number of electrons, due to the strong ferromagnetic (Hund) coupling [23], it is energetically favorable to promote one electron of the occupied level of the highest energy to the next unoccupied level building a triplet state. When this triplet is well below the other states, the system can be described by the underscreened spin-1 Kondo model, which is exactly solvable by a Bethe ansatz [24, 25]. As a consequence, there is a partial screening of the spin 1 that explains the zero bias Kondo peak observed experimentally in this situation [26–28]. In fact, in real QDs one expects a second screening channel to be active below a characteristic temperature T^* suppressing the conductance for bias voltage V or temperature T such that $eV, kT < kT^*$ [29, 30]. However, comparison with experiment suggests that T^* (which depends exponentially on a small coupling constant [30]) is very small, so that one can assume an effective one-channel model for practical purposes [30, 31]. When a gate voltage induces a change in the occupation in such a way that the lowest state of the isolated dot changes from a triplet to a doublet (or conversely), the appropriate model has the form of a generalized Anderson model which has been used to describe valence fluctuation between two magnetic configurations [32–34]. Its impurity version was also solved with a Bethe ansatz [2, 35, 36]. In contrast to the OAM (which has a singlet ground state), its ground state is a doublet.

The physical picture becomes more complex and also more interesting when singlet and triplet states of the configuration with even number of electrons in the dot lie close in energy and neither one of them can be neglected (see figure 1). We call the model that describes the fluctuations between these states and an odd-particle doublet, the singlet–triplet Anderson model (STAM). Again, rigorous results for this model can be borrowed from previous studies of intermediate valence systems. Allub and Aligia proposed the model to describe the low energy physics of Tm impurity fluctuation between the $4f^{12}$ and $4f^{13}$ configurations in a cubic crystal field [37]. Using the numerical renormalization group (NRG) the authors found a singlet or a doublet ground state, depending on the parameters. Therefore, the system has a quantum phase transition when the wavefunction is forced to evolve continuously between these two competing ground states.

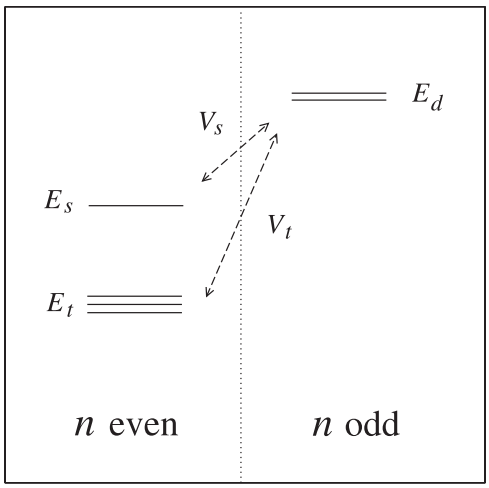

Figure 1. Scheme of the lowest lying levels of the STAM: a doublet (a singlet and a triplet) for the configuration with an odd (even) number of particles n.

Quantum phase transitions are another topic of great interest in condensed matter physics [38]. Recently, Roch *et al* performed several transport measurements through a C_{60} QD with even occupancy inserted in a nanoscale constriction [39]. They were able to tune the parameters in such a way that a clear manifestation of the above-mentioned quantum phase transition was observed. The differential conductance dI/dV as a function of temperature and bias voltage has been measured on both sides of the transition [39]. On the singlet side, a dip in the conductance at $V = 0$ is observed in agreement with theoretical expectations on models similar to the STAM [31, 40, 41] as well as nonequilibrium measurements performed in carbon nanotubes [41]. On the other side of the transition, dI/dV as a function of V shows a structure with three peaks that has not been quantitatively explained yet. We have obtained recently a symmetric three-peak structure [42], but the source of the observed asymmetry remains to be investigated. As the temperature T is decreased, the zero bias conductance $G(T)$ first increases, then it shows a shoulder or a plateau and then increases again. The authors state that this behavior is not understood and speculate that the increase at the lowest temperatures might be due to the opening of another parallel transport mode [39]. This plateau in the conductance was presented by us in a short paper [42].

Recently, a comprehensive study of the physics of a two-level quantum dot, using NRG, has been presented [31]. This model contains the STAM as a limiting case, when higher energy states can be neglected. The advantage of the STAM is that it has fewer parameters and is the minimal model to describe the quantum phase transition when charge fluctuations

are allowed. An important result of the work of Logan *et al* is the derivation of an extended Friedel–Luttinger sum rule which relates the occupation of the dot to the zero bias conductance at very small temperatures [31]. However, in this work, results at finite bias were obtained using approximate expressions and the equilibrium spectral density and (as in previous works) the results do not provide an interpretation of the above-mentioned experimental findings of Roch *et al*. Because of the difficulties in extending robust techniques to the nonequilibrium case (discussed, for example, in [42] and [43]), very few studies of this problem for finite bias voltage exist [41, 42].

In this paper, we present several analytical results which shed light on the behavior of the conductance near the quantum phase transition. We also present numerical results obtained using the non-crossing approximation (NCA), which provide an interpretation of the recent experiments of equilibrium and nonequilibrium conductance in C_{60} QDs near the quantum phase transition [39].

In section 2 we explain the model and its application to multilevel QDs. In section 3 we derive the integer valence limits of the model by means of canonical transformations, and use known results of the ensuing effective models to predict the behavior of the conductance at both sides of the quantum phase transition. The self-consistent system of equations of the NCA approximation and the expression that gives the current through a system described by the model are presented in section 4. In section 5 we describe how the STAM for a particular set of quantum critical points, can be mapped into an OAM plus a free spin, and derive useful results from this mapping. In particular a formula is derived, which allows one to calculate the spectral densities of the STAM in terms of those of the OAM. We also show that the NCA equations satisfy exact results derived from this mapping. Section 6 contains the numerical results obtained with the NCA, and comparison with experiment and previous works. Section 7 is a summary and discussion.

2. The model

2.1. The mixed valence impurity

As originally derived for Tm impurities in a cubic crystal field [37], the STAM hybridizes the lowest states of the $4f^{12}$ configuration, a Γ_1 singlet and Γ_4 triplet, with a doublet (Γ_6 or Γ_7) of the $4f^{13}$ configuration. The fact that only two neighboring configurations are allowed implies that infinite Coulomb repulsion U is assumed. This assumption is taken in all models discussed in this paper. Using the notation $|SM\rangle$, where S is the spin and M its projection, we represent the states of the $4f^{12}$ configuration, as $|00\rangle$ for the singlet and $|1M\rangle$, ($M = -1$, 0 or 1) for the triplet. The doublet is denoted by its spin-1/2 projection $|\sigma\rangle$.

The Hamiltonian can be written in the form

$$H = E_s|00\rangle\langle 00| + E_t \sum_M |1M\rangle\langle 1M| + E_d \sum_\sigma |\sigma\rangle\langle\sigma| + H_{\rm band} + H_{\rm mix}, \quad (1)$$

where $H_{\rm band}$ is a band of extended states:

$$H_{\rm band} = \sum_{k\sigma} \epsilon_k c^\dagger_{k\sigma} c_{k\sigma}, \quad (2)$$

and $H_{\rm mix}$ is the hybridization. In the following we assume k independent matrix elements. Extensions to a more general case are straightforward within the NCA [44, 45]. We can also assume full rotational symmetry and then the form of $H_{\rm mix}$ is determined by Clebsch–Gordan coefficients [2]. Calling $c^\dagger_\sigma = \sum_k c^\dagger_{k\sigma}/\sqrt{N}$ one obtains

$$H_{\rm mix} = \{[V_s|\uparrow\rangle\langle 00| - V_t(|\uparrow\rangle\langle 10| + \sqrt{2}|\downarrow\rangle\langle 1-1|)]c_\uparrow + [V_s|\downarrow\rangle\langle 00| + V_t(|\downarrow\rangle\langle 10| + \sqrt{2}|\uparrow\rangle\langle 11|)]c_\downarrow + \text{h.c.}\}. \quad (3)$$

Performing an electron–hole transformation $h_\uparrow = -c^\dagger_\downarrow$, $h_\downarrow = c^\dagger_\uparrow$, $H_{\rm mix}$ takes the equivalent form

$$H_{\rm mix} = \{V_s(h^\dagger_\uparrow|\downarrow\rangle - h^\dagger_\downarrow|\uparrow\rangle)\langle 00| + V_t[(h^\dagger_\uparrow|\downarrow\rangle + h^\dagger_\downarrow|\uparrow\rangle)\langle 10| + \sqrt{2}(h^\dagger_\uparrow|\uparrow\rangle\langle 11| + h^\dagger_\downarrow|\downarrow\rangle\langle 1-1|)] + \text{h.c.}\}, \quad (4)$$

which is more transparent: the states $|\sigma\rangle$ may be thought as having one particle (4f hole in the Tm case) and when another particle comes from the band, a localized two-particle singlet $|00\rangle$ or a component of the triplet $|1M\rangle$ is formed. In any case, it is clear that the above transformation allows us to treat with the same Hamiltonian the cases in which the configuration with the doublet has either one more particle or one less particle than the other one.

We can assume that $V_s > 0$ changing, if necessary, the phase of $|00\rangle$. Similarly we assume $V_t > 0$. For $E_t \to +\infty$, the model reduces to the OAM. For $E_s \to +\infty$, the model describes valence fluctuations between two magnetic configurations [2, 32]. In both limits, for constant density of conduction states, the model is exactly solvable (by the Bethe ansatz) and the ground state is a singlet (doublet) in the first (second) case [2, 35, 36]. Thus, the model has a quantum phase transition as a function of $E_s - E_t$. The position of the transition depends on the other parameters of the model, leading to a quantum critical surface that can be determined by calculating the magnetic susceptibility at $T \to 0$ using the numerical renormalization group (NRG) [37]. However, as shown in section 5, if $V_t = V_s$, the transition takes place exactly at $E_s - E_t = 0$, independently of the value of E_d. In addition, along this quantum critical line[3], the model can be mapped into an OAM plus a free spin 1/2.

2.2. The multilevel dot

In a dot hybridized with two leads, the triplet is formed from the singlet with lowest energy by promoting an electron from the highest occupied level, which we denote as a, to the highest unoccupied level b. One can restrict to these two levels. The states of these two levels are hybridized with the bands of the two leads, left ($\nu = $ L) and right ($\nu = $ R) described by

$$H_{\rm band} = \sum_{\nu k\sigma} \epsilon_{\nu k} h^\dagger_{\nu k\sigma} h_{\nu k\sigma}, \quad (5)$$

[3] In the space of free parameters of the model, at zero temperature and equilibrium, the set of all quantum critical points forms a two-dimensional surface. Fixing either $V_s = V_t$ or $E_s = E_t$ defines the same quantum critical line on this surface.

through the following term in the Hamiltonian:

$$H_{\rm mix} = \sum_{\nu\sigma}[(V_\nu^a a_\sigma^\dagger + V_\nu^b b_\sigma^\dagger)h_{\nu\sigma} + \text{h.c.}], \tag{6}$$

where $h_{\nu\sigma}^\dagger = \sum_k h_{\nu k\sigma}^\dagger/\sqrt{N}$. We assume $V_{\rm L}^a V_{\rm R}^b = V_{\rm L}^b V_{\rm R}^a$, so that only one conduction channel

$$h_\sigma = \left(\sum_\nu V_\nu^\eta h_{\nu\sigma}\right)/[(V_{\rm L}^\eta)^2 + (V_{\rm R}^\eta)^2]^{1/2} \qquad (\eta = a \text{ or } b) \tag{7}$$

hybridizes with the dot states. In general, the orthogonal linear combination of $h_{\nu\sigma}$ also plays a role and 'screens' the remaining doublet ground state when the localized triplet is well below the singlet, leading to a singlet ground state [29, 30]. However, as mentioned in section 1, the characteristic energy scale involved in this second screening T^* might be exponentially small. As argued before [30], this is likely the case of previous experiments. As our results will show (section 6), the one-channel case also describes the recent transport measurements in C_{60} QDs [39]: the theory in the more general two-channel case [29, 30, 46] predicts that the zero bias conductance $G(T)$ should decrease at very low temperatures and $\mathrm{d}I/\mathrm{d}V$ should also decrease for the smallest applied bias voltages V in contrast to the observations. This indicates that T^* is smaller than the smallest temperature in the experiments.

Assuming that the difference between the energies of the levels b and a is larger than the hybridization terms, one can retain only the lowest doublet and neglect the singlets that contain at least one particle in the state b. Then, performing an electron–hole transformation if necessary, the relevant low energy states of the dot are

$$|\sigma\rangle = a_\sigma^\dagger|0\rangle, \qquad |00\rangle = a_\uparrow^\dagger a_\downarrow^\dagger|0\rangle, \qquad |11\rangle = b_\uparrow^\dagger a_\uparrow^\dagger|0\rangle,$$
$$|10\rangle = \frac{1}{\sqrt{2}}(b_\uparrow^\dagger a_\downarrow^\dagger + b_\downarrow^\dagger a_\uparrow^\dagger)|0\rangle, \qquad |1-1\rangle = b_\downarrow^\dagger a_\downarrow^\dagger|0\rangle. \tag{8}$$

The triplet states should be kept because the ferromagnetic exchange may render them the lowest of the configuration with an even number of particles [23, 26–28, 39] (see figure 1). Restricting the action of the fermion operators to these six states one has

$$a_\uparrow^\dagger = |00\rangle\langle\downarrow|, \qquad b_\uparrow^\dagger = |11\rangle\langle\uparrow| + |10\rangle\langle\downarrow|/\sqrt{2},$$
$$a_\downarrow^\dagger = -|00\rangle\langle\uparrow|, \qquad b_\downarrow^\dagger = |1-1\rangle\langle\downarrow| + |10\rangle\langle\uparrow|/\sqrt{2}. \tag{9}$$

Replacing equations (7) and (9) in equation (6) one obtains equation (4) with

$$V_s = [(V_{\rm L}^a)^2 + (V_{\rm R}^a)^2]^{1/2},$$
$$V_t = [(V_{\rm L}^b)^2 + (V_{\rm R}^b)^2]^{1/2}/\sqrt{2}. \tag{10}$$

Therefore, at equilibrium, the model takes the same form as equation (1). The values of E_s, E_t and E_d are easily determined from the on-site energies and correlations at the QD, including Hund exchange [31]. The nonequilibrium case is discussed in sections 4.2 and 4.

3. The integer valence limits

When $|\min(E_s, E_t) - E_d| \gg \max(V_s, V_t)$, the model is at the integer valence (or 'Kondo') limit and a Hamiltonian of the exchange type can be derived, using a canonical transformation which eliminates $H_{\rm mix}$ from the Hamiltonian and originates a term quadratic in $H_{\rm mix}$ [7, 47]. Two cases can be distinguished, depending on which configuration is favored.

3.1. Odd number of electrons

For $\min(E_s, E_t) - E_d \gg \max(V_s, V_t)$, the doublet is favored. In this case, the canonical transformation is a particular case of that considered in [21] for a Cr trimer on Au(111) (a doublet ground state with virtual charge fluctuations to singlets and triplets). Using equations (1), (2) and (4), one obtains

$$H_{\rm odd} = \sum_{k\sigma} -\epsilon_k h_{k\sigma}^\dagger h_{k\sigma} + (F_s - 3F_t)h_\sigma^\dagger h_\sigma + J\mathbf{s}\cdot\mathbf{S},$$
$$J = 4(F_s - F_t), \qquad F_\eta = \frac{V_\eta^2}{2(E_\eta - E_d)}, \tag{11}$$

where $\mathbf{s} = \sum_{\alpha\beta} h_\alpha^\dagger \boldsymbol{\sigma}_{\alpha\beta} h_\beta/2 = \sum_{\alpha\beta} c_\alpha^\dagger \boldsymbol{\sigma}_{\alpha\beta} c_\beta/2$ is the spin of the conduction electrons at the QD and similarly $\mathbf{S}$ is the spin of the doublet. This is a Kondo model with potential scattering (second term of equations (11)). It is known from NRG that, when J is positive, it is a marginally relevant perturbation (it grows with renormalization to $J \to +\infty$) leading to a singlet ground state [37, 48]. Instead for negative J, the exchange term is marginally irrelevant ($J \to 0$) and the ground state is a doublet. Therefore, there is a quantum phase transition for $J = 0$, or $F_s = F_t$ in terms of the parameters of the original model.

Moreover, at both sides of the transition, the system is a Fermi liquid, but the phase shift at the Fermi energy is $\delta = \pi/2$ for $J > 0$, but $\delta = 0$ for $J < 0$. For the one-channel case that we are considering, this means that the zero bias conductance is maximum (vanishing) for $J > 0$ ($J < 0$) [29]. Therefore, there is a jump in the conductance at the quantum phase transition. This is in agreement with recent NRG results and an analysis of a generalized Friedel–Luttinger sum rule [31].

Note that, for $V_s = V_t$, the transition is exactly at $E_s = E_t$. It has been found by NRG that this statement is valid for any occupation of the dot and not only for integer occupation [37]. An analytic argument which supports this numerical result is given in section 5.2.

3.2. Even number of electrons

For $E_d - \min(E_s, E_t) \gg \max(V_s, V_t)$, if in addition $|E_s - E_t| \gg \max(V_s, V_t)$, the highest lying levels between the singlet and the triplet can be neglected, and the resulting effective model reduces to one of the cases considered in [2]. In particular, if the triplet is the lowest in energy one has the underscreened Kondo model with singular Fermi liquid behavior [25].

The effective model $H_{\rm even}$ is reached when E_s lies near E_t. In the following we assume that both energies lie well below E_d. In order to obtain a more transparent form of $H_{\rm even}$ we

introduce two fictitious spins 1/2, $\mathbf{S}_1$ and $\mathbf{S}_2$, to represent the states of the configuration with even number of particles, in terms of the states of these two spins $|\sigma_1\sigma_2\rangle$ as follows:

$$|00\rangle = (|\uparrow\downarrow\rangle - |\downarrow\uparrow\rangle)/\sqrt{2}, \qquad |11\rangle = |\uparrow\uparrow\rangle,$$
$$|10\rangle = (|\uparrow\downarrow\rangle + |\downarrow\uparrow\rangle)/\sqrt{2}, \qquad |1-1\rangle = |\downarrow\downarrow\rangle. \tag{12}$$

The resulting effective Hamiltonian is

$$H_{\rm even} = \sum_{k\sigma} \epsilon_k c^\dagger_{k\sigma} c_{k\sigma} + \frac{2V_t^2}{E_d - E_t}\mathbf{s}\cdot(\mathbf{S_1}+\mathbf{S_2}) + (E_t - E_s)(\mathbf{S_1}\cdot\mathbf{S_2}) + V_sV_t\left(\frac{1}{E_d - E_s} + \frac{1}{E_d - E_t}\right) \times \mathbf{s}\cdot(\mathbf{S_1}-\mathbf{S_2}) - \frac{V_t^2}{E_d - E_t}n_0 + \left(\frac{V_t^2}{E_d - E_t} - \frac{V_s^2}{E_d - E_s}\right)n_0 n_S, \tag{13}$$

where $n_0 = c^\dagger_\sigma c_\sigma$ and $n_S = |00\rangle\langle 00| = 1/4 - \mathbf{S_1}\cdot\mathbf{S_2}$.

For $V_s = 0$ and E_t well below E_s, $H_{\rm even}$ reduces to the spin-1 underscreened Kondo model plus potential scattering. This model has a doublet ground state and singular Fermi liquid behavior [25]. A Hamiltonian with the first four terms (the most relevant ones) was studied by NRG and found to have a singlet–doublet quantum phase transition which is in general continuous of the Kosterlitz–Thouless type [49], as the original model [37]. The transition is first order only in the particular case in which the fourth term (proportional to $\mathbf{S}_1 - \mathbf{S}_2$) vanishes [49]. This implies either $V_s = 0$ or $V_t = 0$ in our model. Note that, for $V_s = V_t$ and $E_s = E_t$, the spin $\mathbf{S}_2$ decouples and the spin $\mathbf{S}_1$ has a usual Kondo interaction with the band and is therefore screened. An analysis of the strong coupling fixed point for the STAM [37] and for $H_{\rm even}$ without the terms proportional to n_0 [49] indicates that a generic feature of the phase with a doublet ground state (and also the quantum critical point) is a free spin 1/2 and a Kondo screened spin 1/2 at low temperatures. This implies a phase shift $\delta = \pi/2$ and maximum conductance G, as in the phase with a singlet ground state when the configuration with an odd number of particles is favored (see section 3.1).

Starting at the transition and decreasing E_s, the remaining spin is also screened in a second stage and the ground state is a singlet. The full Fermi liquid behavior is restored, and one expects $\delta = G = 0$. Another way of thinking on this is that the screening of the remaining spin leads to a Fano antiresonance with a characteristic energy scale given by the second stage Kondo effect (see section 5.2).

Note that the jump in the conductance at the transition takes place in spite of the fact that the transition is continuous (as discussed above) and not first order. The impurity contribution to the magnetic susceptibility also jumps at zero temperature at the transition [37, 49].

These results for the conductance agree with direct calculations using NRG [31, 40]

4. The non-crossing approximation (NCA)

4.1. Representation of the Hamiltonian with slave particles

The NCA has been used to study the OAM out of equilibrium [51]. To extend this formalism to the STAM, we introduce auxiliary bosons, one for the singlet state (s) and three for the triplets (t_M, $M = -1, 0, 1$), and auxiliary fermions (f_σ) for the doublet, in analogy to the $SU(N) \times SU(M)$ generalization of the Anderson model [52, 53]. In terms of the auxiliary operators, the Hamiltonian takes the form

$$H = E_s s^\dagger s + E_t \sum_M t^\dagger_M t_M + E_d \sum_\sigma f^\dagger_\sigma f_\sigma + \sum_{\nu k\sigma} \epsilon_{\nu k} c^\dagger_{\nu k\sigma} c_{\nu k\sigma} + \sum_{\nu k\sigma}[(V^s_\nu d^\dagger_{s\sigma} + V^t_\nu d^\dagger_{{\rm t}\sigma})c_{\nu k\sigma} + {\rm h.c.}], \tag{14}$$

($\nu = {\rm L}$ or R), where $E_f = E_d$ and

$$d^\dagger_{s\sigma} = f^\dagger_\sigma s, \qquad d^\dagger_{{\rm t}\uparrow} = -(f^\dagger_\uparrow t_0 + \sqrt{2} f^\dagger_\downarrow t_{-1})/\sqrt{3}, \qquad d^\dagger_{{\rm t}\downarrow} = (f^\dagger_\downarrow t_0 + \sqrt{2} f^\dagger_\uparrow t_1)/\sqrt{3}, \tag{15}$$

with the constraint

$$s^\dagger s + \sum_M t^\dagger_M t_M + \sum_\sigma f^\dagger_\sigma f_\sigma = 1. \tag{16}$$

The factor $1/\sqrt{3}$ in equations (15) was chosen to give a more symmetric form for the NCA equations, in particular near the quantum critical line for which the system is exactly solvable (see section 5.4). Comparing with equations (9), one can realize that $d^\dagger_{s\uparrow} = -a_\downarrow$, $d^\dagger_{s\downarrow} = a_\uparrow$, $d^\dagger_{{\rm t}\uparrow} = -\sqrt{2/3}b_\downarrow$ and $d^\dagger_{{\rm t}\downarrow} = \sqrt{2/3}b_\uparrow$. The representation of equation (14) was chosen in such a way that if the triplet can be neglected (because either $E_t \to +\infty$ or $V^t_{\rm L} = V^t_{\rm R} = 0$), the model reduces to the OAM.

As in section 2.2, the mixing part of equation (14) can be put in the form of equation (3) with $V_s = [(V^s_{\rm L})^2 + (V^s_{\rm R})^2]^{1/2}$ and $V_t = [(V^t_{\rm L})^2 + (V^t_{\rm R})^2]^{1/2}/\sqrt{3}$.

4.2. Equation for the current

For the calculation of the current, we consider a multilevel QD with at most six relevant states of the Hilbert space, as described in section 2.2 (see equations (8)). For the case of proportionate couplings of the relevant two levels ($V^a_{\rm L}V^b_{\rm R} = V^b_{\rm L}V^a_{\rm R}$ as we are assuming), Meir and Wingreen [50] provided an expression for the current in a nonequilibrium situation (equation (9) of [50]), which is given by a trace of $\mathbf{\Gamma G}^{\rm r}$, where $\mathbf{\Gamma}$ is given in terms of V^η_ν and $\mathbf{G}^{\rm r}$ is a matrix of retarded Green's functions. In our case, $\mathbf{\Gamma}$ and $\mathbf{G}^{\rm r}$ are 4×4 matrices in spin and level (a or b) indices. It is easy to see that the product $\mathbf{\Gamma G}^{\rm r}$ is the same (as it should be) in the representation of slave particles used above (equations (15)), in which the index η refers to s and t instead of a and b (the normalization factors in $\mathbf{\Gamma}$ and $\mathbf{G}^{\rm r}$ cancel).

$\mathbf{\Gamma}$ is diagonal in the spin index. Within the NCA, the expectation values entering the Green's functions decouple into fermion and boson parts [51] and both are diagonal as a

consequence of $SU(2)$ invariance of the Hamiltonian. This means that $\mathbf{G}^{\mathrm{r}}$ is diagonal in level index. This allows us to simplify the resulting expression, which takes the form

$$I = \frac{A\pi e}{h}\int \mathrm{d}\omega \sum_{\eta} \Gamma^{\eta}\rho_d^{\eta}(\omega)[f_{\mathrm{L}}(\omega) - f_{\mathrm{R}}(\omega)], \tag{17}$$

where $\rho_d^{\eta}(\omega) = -\operatorname{Im} G^{\mathrm{r}}_{\mathrm{d}\eta\sigma}(\omega)/\pi$ is the spectral density of $d^{\dagger}_{\eta\sigma}$:

$$\Gamma^{\eta} = \Gamma^{\eta}_{\mathrm{R}} + \Gamma^{\eta}_{\mathrm{L}}, \qquad \text{with } \Gamma^{\eta}_{\nu} = 2\pi \sum_k |V^{\eta}_{\nu}|^2 \delta(\omega - \epsilon_k) \tag{18}$$

assumed independent of ω within a bandwidth D and zero elsewhere:

$$A = 4\Gamma^{\eta}_{\mathrm{R}}\Gamma^{\eta}_{\mathrm{L}}/(\Gamma^{\eta}_{\mathrm{R}} + \Gamma^{\eta}_{\mathrm{L}})^2 \leqslant 1 \tag{19}$$

(independent of η) is a parameter that characterizes the asymmetry between left and right leads, and $f_{\nu}(\omega)$ is the Fermi function with the chemical potential μ_{ν} of the corresponding lead.

4.3. Spectral densities and Green's functions

The spectral densities of the operators $d^{\dagger}_{\eta\sigma}$ defined by equations (15) for given spin, $\rho_d^s(\omega)$ and $\rho_d^t(\omega)$, are determined by convolutions from those of the auxiliary particles $\rho_{\lambda}(\omega)$ with the lesser Green's functions $G^{<}_{\lambda}(\omega)$ ($\lambda = s$, t, or f) as follows:

$$\rho_d^{\eta}(\omega) = \frac{1}{Z}\int \mathrm{d}\omega' (G^{<}_{\eta}(\omega')\rho_f(\omega'+\omega) + G^{<}_{f}(\omega'+\omega)\rho_{\eta}(\omega')), \tag{20}$$

$$Z = \int \mathrm{d}\omega (G^{<}_{s}(\omega) + 2G^{<}_{f}(\omega) + 3G^{<}_{t}(\omega)), \tag{21}$$

where we define $G^{<}_{t}(\omega)$ as the Fourier transform of $\langle t^{\dagger}_M(0)t_M(t)\rangle$ (the result is independent of M because of $SU(2)$ symmetry) and similarly for $G^{<}_{s}(\omega)$ and $G^{<}_{f}(\omega)$. The spectral densities of the auxiliary particles are given by the imaginary part of the corresponding retarded Green's function as usual: $\rho_{\lambda}(\omega) = -\operatorname{Im} G^{\mathrm{r}}_{\lambda}(\omega)/\pi$. In turn, these Green's functions

$$G^{\mathrm{r}}_{\lambda}(\omega) = \frac{1}{\omega - E_{\lambda} - \Sigma^{\mathrm{r}}_{\lambda}(\omega)}, \tag{22}$$

are given in terms of retarded self-energies $\Sigma^{\mathrm{r}}_{\lambda}(\omega)$, which as in the case of the OAM [51], should be determined self-consistently. The imaginary parts are given by the following set of integral equations:

$$\begin{aligned}
\operatorname{Im}\Sigma^{\mathrm{r}}_{s}(\omega) &= -\int \mathrm{d}\omega'\, \Gamma^{s}\rho_f(\omega')\tilde{f}(\omega'-\omega),\\
\operatorname{Im}\Sigma^{\mathrm{r}}_{t}(\omega) &= -\tfrac{1}{3}\int \mathrm{d}\omega'\, \Gamma^{t}\rho_f(\omega')\tilde{f}(\omega'-\omega),\\
\operatorname{Im}\Sigma^{\mathrm{r}}_{f}(\omega) &= -\tfrac{1}{2}\int \mathrm{d}\omega' [\Gamma^{s}\rho_s(\omega') + \Gamma^{t}\rho_t(\omega')]\tilde{h}(\omega-\omega'),
\end{aligned} \tag{23}$$

where

$$\begin{aligned}
\tilde{f}(\omega) &= [\Gamma^{\eta}_{\mathrm{L}} f_{\mathrm{L}}(\omega) + \Gamma^{\eta}_{\mathrm{R}} f_{\mathrm{R}}(\omega)]/\Gamma^{\eta},\\
\tilde{h}(\omega) &= [\Gamma^{\eta}_{\mathrm{L}}(1 - f_{\mathrm{L}}(\omega)) + \Gamma^{\eta}_{\mathrm{R}}(1 - f_{\mathrm{R}}(\omega))]/\Gamma^{\eta},
\end{aligned} \tag{24}$$

and Γ^{η}_{ν}, Γ^{η} ($\eta = s$ or t) are given by equations (18). The real part of the self-energies are obtained using Kramers–Kronig relations:

$$\operatorname{Re}\Sigma^{\mathrm{r}}_{\lambda}(\omega) = \frac{1}{\pi}\mathcal{P}\int \mathrm{d}\omega' \frac{\operatorname{Im}\Sigma^{\mathrm{r}}_{\lambda}(\omega')}{\omega' - \omega}. \tag{25}$$

Once the retarded self-energies are obtained solving the above system of equations, the lesser Green's functions come from the solution of the following integral equations:

$$G^{<}_{d}(\omega) = |G^{\mathrm{R}}_{d}(\omega)|^2 \Sigma^{<}_{d}(\omega), \tag{26}$$

$$\begin{aligned}
\Sigma^{<}_{s}(\omega) &= \frac{1}{\pi}\int \mathrm{d}\omega'\, \Gamma^{s} G^{<}_{f}(\omega')\tilde{h}(\omega'-\omega),\\
\Sigma^{<}_{t}(\omega) &= \frac{1}{3\pi}\int \mathrm{d}\omega'\, \Gamma^{t} G^{<}_{f}(\omega')\tilde{h}(\omega'-\omega),\\
\Sigma^{<}_{f}(\omega) &= \frac{1}{2\pi}\int \mathrm{d}\omega' [\Gamma^{s} G^{<}_{s}(\omega') + \Gamma^{t} G^{<}_{t}(\omega')]\tilde{f}(\omega-\omega').
\end{aligned} \tag{27}$$

4.4. Numerical details

In the numerical procedure to solve the NCA equations, we have used a set of self-adjusting meshes (rather than the fixed one used in [53]) to describe the spectral densities and lesser Green's functions of the auxiliary particles: we have evaluated $\rho_{\lambda}(\omega)$ and $G^{<}_{\lambda}(\omega)$ in the corresponding logarithmic array of discrete frequencies ω_{λ}, built in each iteration in order to have a larger density of points near the corresponding peaks or singularities of these functions. The procedure guarantees the resolution of the sets of integral equations (23) and (27) to a high degree of accuracy. To calculate the spectral densities, $\rho_d^s(\omega)$ and $\rho_d^t(\omega)$, we have used two different logarithmic meshes centered at the peaks of the functions entering equation (20). This scheme of numerical resolution allows us to obtain the conductance at both sides of the transition, within equilibrium and nonequilibrium, and for all values of the parameters considered.

The logarithmic discretization is similar to that used in NRG calculations, where only one mesh centered at the Fermi energy $\mu_{\mathrm{L}} = \mu_{\mathrm{R}}$ and with an arbitrarily large number of frequencies near this energy is used [54].

5. The exactly solvable case

For $V_s = V_t$ and $E_s = E_t$, the model given by equations (1)–(3) or (4) has additional symmetries and is exactly solvable [37]. It has been shown numerically that these equations define a quantum critical line (a point for each value of E_d/V_s) (see footnote 3) that separates regions of singlet and double ground states [37]. In this section we provide simple analytical arguments to demonstrate these results, map the corresponding spectral densities and show that the NCA is consistent with these results.

5.1. The STAM on the quantum critical line

In analogy to equations (12), let us consider a (probably fictitious) system, like the two-level one considered in section 2.2, but in which the relevant singlet is $|00\rangle = (1/\sqrt{2})(b^\dagger_\uparrow a^\dagger_\downarrow - b^\dagger_\downarrow a^\dagger_\uparrow)|0\rangle$ (instead of $a^\dagger_\uparrow a^\dagger_\downarrow|0\rangle$, see equations (8)), and with the mixing term

$$H_{\rm mix} = \sum_{\nu\sigma}[V^b_\nu b^\dagger_\sigma h_{\nu\sigma} + \text{h.c.}], \tag{28}$$

which does not involve the $a^\dagger_\sigma$ and a_σ operators. Clearly, the resulting model (equation (31) with $E_t = E_s$) is the OAM with infinite Coulomb repulsion U for the level b (which is exactly solvable by Bethe ansatz [2]), while level a within the relevant Hilbert subspace (equations (8) with $|00\rangle$ replaced as above) reduces to a decoupled spin 1/2: $|\sigma\rangle = a^\dagger_\sigma|0\rangle$. Within this subspace

$$\begin{aligned} b^\dagger_\uparrow &= |11\rangle\langle\uparrow| + (|10\rangle\langle\downarrow| + |00\rangle\langle\downarrow|)/\sqrt{2}, \\ b^\dagger_\downarrow &= |1-1\rangle\langle\downarrow| + (|10\rangle\langle\uparrow| - |00\rangle\langle\uparrow|)/\sqrt{2}. \end{aligned} \tag{29}$$

Replacing these equations in equation (28) one obtains equation (4) with

$$V_s = V_t = [(V^b_{\rm L})^2 + (V^b_{\rm R})^2]^{1/2}/\sqrt{2}. \tag{30}$$

This shows the equivalence of the STAM for $V_s = V_t$ and $E_s = E_t$ with an OAM plus a free doublet.

5.2. Effect of singlet–triplet splitting

Proceeding as above, it is easy to see that for $V_s = V_t = V_{\rm OAM}/\sqrt{2}$, but arbitrary E_s and E_t, the STAM given by equations (1), (2) and (4), except for an irrelevant constant, is mapped onto

$$\begin{aligned} H' = &\sum_{k\sigma} -\epsilon_k h^\dagger_{k\sigma} h_{k\sigma} + (E_t - E_d)\sum_\sigma b^\dagger_\sigma b_\sigma \\ &+ \sum_\sigma [V_{\rm OAM} b^\dagger_\sigma h_\sigma + \text{h.c.}] + U b^\dagger_\uparrow b_\uparrow b^\dagger_\downarrow b_\downarrow \\ &+ (E_t - E_s)(\mathbf{S}_a \cdot \mathbf{S}_b - 1/4), \end{aligned} \tag{31}$$

where $U \to +\infty$, $\mathbf{S}_a$ is the spin operator of the spin 1/2 which is free for $E_t = E_s$, and similarly $\mathbf{S}_b = \sum_{\alpha\beta} b^\dagger_\alpha \boldsymbol{\sigma}_{\alpha\beta} b_\beta/2$.

For $E_t = E_s$, clearly $\mathbf{S}_b$ is screened as usual in the OAM and the ground state is a doublet which is the direct product of a Fermi liquid singlet times the spin state $|\sigma\rangle$. If the state b is hybridized with two conducting leads (as above), the physics of the OAM determines that the conductance $G = G_0 \sin^2\delta$, with $G_0 = 2e^2A/h$ and $\delta = \pi\langle\sum_\sigma b^\dagger_\sigma b_\sigma\rangle/2$ [55]. In particular when the total number of particles $\langle\sum_\sigma b^\dagger_\sigma b_\sigma\rangle + 1 = 2$, one has maximum conductance, in agreement with the result discussed in section 3.2.

When the last term of equation (31) is added, one can think of $\mathbf{S}_b$ as representing the spin of itinerant electrons in an effective heavy mass Fermi liquid at low energies. In fact, comparison of a mean-field slave-boson treatment with NRG calculations [56] show that this picture is qualitatively correct[4] for $\langle\sum_\sigma b^\dagger_\sigma b_\sigma\rangle + 1 \simeq 2$. Then, as discussed in section 3, from the physics of the ensuing effective Kondo model [48, 56], when $E_t < E_s$ (ferromagnetic coupling) the exchange interaction renormalizes to zero and the ground state continues to be a doublet, while for $E_t > E_s$ a second screening takes place and the ground state is a singlet. This results agrees with previous NRG results [37] and confirms that $V_s = V_t$ and $E_s = E_t$ correspond to the quantum critical line.

If the OAM for $E_t = E_s$ is in the Kondo regime ($\langle\sum_\sigma b^\dagger_\sigma b_\sigma\rangle \simeq 1$), one expects that addition of a positive exchange ($E_t > E_s$) induces a Fano–Kondo antiresonance, depressing the conductance at low temperatures [55, 56], while nothing dramatic happens for $E_t < E_s$. This again agrees with the results of section 3.

While as discussed above, the ground state is a doublet for $E_t < E_s$, we remind the reader that for realistic two-level systems at low enough temperatures ($T < T^*$, see section 2.2) a second screening channel should become active, leading to a screening of the remaining doublet and a decrease in the conductance [29, 30, 46].

5.3. Mapping of the spectral densities

Since the OAM out of equilibrium has been studied before [43, 51, 57–59][5], results for the conductance of the OAM can be extended to the STAM on the quantum critical line if one knows how to express the spectral densities $\rho^s_d(\omega)$ and $\rho^t_d(\omega)$ of the operators $d^\dagger_{s\sigma}$, $d^\dagger_{t\sigma}$ of the STAM (see equations (15)), which enter the equation for the current (17), in terms of the spectral density $\rho_b(\omega)$ of the operator $b^\dagger_\sigma$ of the OAM (included in equation (31) for $E_t = E_s$). These densities are proportional to the imaginary part of the corresponding retarded Green's functions. For example, $\rho_b(\omega) = -\,\text{Im}\,G^{\rm r}_b(\omega)$, where $G^{\rm r}_b(\omega)$ is the Fourier transform of $G^{\rm r}_b(t) = -\text{i}\theta(t)\langle b_\sigma(t)b^\dagger_\sigma + b^\dagger_\sigma b_\sigma(t)\rangle$, where $\theta(t)$ is the step function. The operators $d^\dagger_{s\sigma}$ and $d^\dagger_{t\sigma}$ of the STAM can be expressed in terms of those of the OAM using equations (15) and the mapping of operators explained in section 5.1. For example

$$\begin{aligned} d_{s\downarrow} &= \frac{1}{\sqrt{2}}(b^\dagger_\uparrow a^\dagger_\downarrow - b^\dagger_\downarrow a^\dagger_\uparrow)a_\downarrow, \\ d_{t\downarrow} &= \frac{1}{\sqrt{6}}[2b^\dagger_\uparrow a^\dagger_\uparrow a_\uparrow + (b^\dagger_\uparrow a^\dagger_\downarrow + b^\dagger_\downarrow a^\dagger_\uparrow)a_\downarrow]. \end{aligned} \tag{32}$$

Replacing this in expectation values like $\langle d_{\eta\downarrow}(t)d^\dagger_{\eta\downarrow}\rangle$, one obtains expectation values involving six fermion operators. Four of them correspond to $a^\dagger_\sigma$ and a_σ operators, which have no dynamics (are time-independent) and are decoupled from the remaining $b^\dagger_\sigma$ and b_σ operators. Evaluating the expectation values involving $a^\dagger_\sigma$ and a_σ operators, using spin conservation, $\langle a^\dagger_\uparrow a_\uparrow a^\dagger_\downarrow a_\downarrow\rangle = 0$, and assuming the paramagnetic phase (in particular $\langle a^\dagger_\sigma a_\sigma\rangle = 1/2$), we obtain after some algebra

$$\langle d_{\eta\downarrow}(t)d^\dagger_{\eta\downarrow}\rangle = \tfrac{1}{2}\langle b^\dagger_\sigma b_\sigma(-t)\rangle, \tag{33}$$

[4] Note that the slave-boson mean-field theory is an approximation for the low energy physics and is therefore inadequate to calculate the Luttinger integral $I_{\rm L}$ considered in [31], which involves high energies.

[5] The correct coefficient of $-(eV/\tilde{\Delta})^2$ is $1 + [(2+3A)\tilde{u}^2 - 3A]/4$.

independently of $\eta = s$ or t. Proceeding in the same way for the remaining expectation values we finally obtain

$$\rho_d^s(\omega) = \rho_d^t(\omega) = \tfrac{1}{2}\rho_b(-\omega), \tag{34}$$

which relates the spectral densities of the STAM to that of the OAM on the quantum critical line.

5.4. Mapping of the NCA equations

It is interesting to note that the NCA approach for the STAM described in section 4, and the corresponding one for the OAM, although they seem to be quite different at first glance, can be related and satisfy equations (34). The NCA for the OAM [51] makes use of an auxiliary boson $\tilde{b}$ and auxiliary fermions $\tilde{f}_\sigma$, describing the electron operator as $b_\sigma = \tilde{b}^\dagger \tilde{f}_\sigma$. In analogy to equations (18), the coupling to the right and left leads are described by coupling constants Γ_R and Γ_L. We define the total coupling of the OAM as $\Gamma = \Gamma_R + \Gamma_L$. The mapping between both models described above for $V_s = V_t$ and $E_s = E_t$ implies that $\Gamma_\nu^s = 1/2\Gamma_\nu$, and $\Gamma_\nu^t = 3/2\Gamma_\nu$. Therefore, $\Gamma^t = 3\Gamma^s = 3/2\Gamma$. As a consequence of these relations, the equations for the auxiliary bosons s and those for t_M have the same form (see equations (23) and (27)). Moreover the resulting equations for the self-energies take the same form as those of the auxiliary fermions $\tilde{f}_\sigma$ of the OAM (equation (23) of [51]), but with $f_\nu(\omega)$ replaced by $1 - f_\nu(\omega)$. Similarly, the self-energies of the auxiliary fermions f_σ of the STAM take the same form as those of the auxiliary boson $\tilde{b}$ of the OAM, with the same change as above in the Fermi functions f_ν. This implies the following relations for the auxiliary particles:

$$\rho_s(\omega) = \rho_t(\omega) = \rho_{\tilde{f}}(-\omega), \qquad \rho_f(\omega) = \rho_{\tilde{b}}(-\omega),$$
$$G_s^<(\omega) = G_t^<(\omega) = G_{\tilde{f}}^<(-\omega), \qquad G_f^<(\omega) = G_{\tilde{b}}^<(-\omega). \tag{35}$$

The density $\rho_b(\omega)$ of the real fermion b_σ of the OAM is given by a convolution (equation (21) of [51]) similar to that defining $\rho_d^s(\omega)$ and $\rho_d^t(\omega)$ (equation (20)) with the replacements indicated by equations (35), but with the difference that Z in the denominator is replaced by $Z_{OAM} = \int d\omega (G_{\tilde{b}}^<(\omega) + 2G_{\tilde{f}}^<(\omega))$. Using equations (21) and (35), it is easy to see that $Z = 2Z_{OAM}$. This leads to equations (34) for the relation between spectral densities. We have checked it numerically by an independent solution of the NCA equations for both models.

6. Numerical results

For the numerical solution of the NCA equations, we take $V_s = V_t$, so that, independently of E_d, the quantum transition occurs at the exactly solvable case $E_s = E_t$ described above. We take Γ, the coupling of the OAM involved in the mapping described in the previous section, as the unit of energy. Therefore $\Gamma^s = 1/2\Gamma$, and $\Gamma^t = 3/2\Gamma$. We take the bandwidth of the conduction bands $D = 10\Gamma$. At equilibrium $\mu_L = \mu_R$ and the properties of the model depend on $E_\eta + \mu_L - E_d$ ($\eta = s$ or t) and not separately on the individual parameters. Therefore, without loss of generality, we take $E_d = \mu_L = \mu_R = 0$. Out of equilibrium, unless otherwise stated, we assume $\Gamma_R^\eta = \Gamma_L^\eta = \Gamma^\eta/2$ and $\mu_L + \mu_R = 0$ (as expected for equal couplings to the left and right leads).

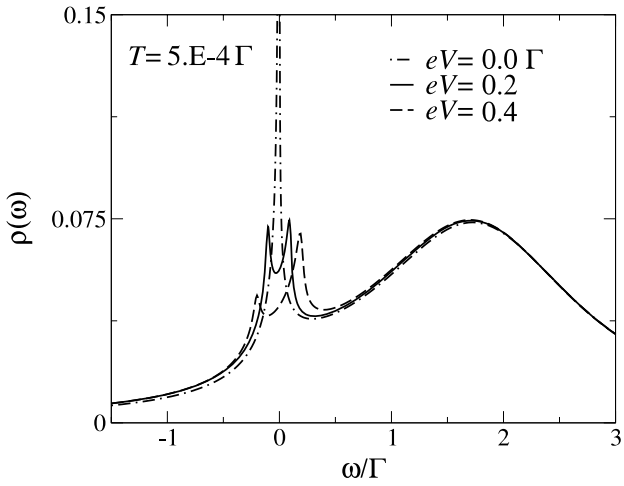

Figure 2. Spectral densities as a function of frequency for $T = 5 \times 10^{-4}$, $E_t = E_s = -2$, and three bias voltages V.

The choice $V_s = V_t$ leaves four free parameters: temperature T, bias voltage V, which determines the difference in chemical potentials $\mu_L - \mu_R = eV$, E_t/Γ (or E_s/Γ) which controls the valence and can be modified by a gate voltage, and finally $(E_s - E_t)/\Gamma$, which controls the distance to the quantum critical line (see footnote 3). This parameter has also been controlled experimentally by Roch *et al* [39]. A great advantage of taking $V_s = V_t$ is that we know exactly where the quantum transition is, while for other ratios V_s/V_t, the position of the transition has to be determined numerically [37]. This is very time consuming within the NCA because it is required to solve the structure of the spectral densities at low temperatures many times near the transition.

In this paper, we restrict our study to $E_s, E_t < E_d$. This means that the configuration with an even number of particles is favored. This situation corresponds to the most novel experimental results, in particular those of Roch *et al* for the conductance through C_{60} QDs near the quantum phase transition [39]. In the following and for the sake of brevity we call the 'singlet side' of the transition the region of parameters with a singlet ground state ($E_s < E_t$ in our case with $V_s = V_t$), and (to be consistent with Roch *et al*) we denote by the 'triplet side' the region $E_s > E_t$ although as explained above, the spin 1 is partially screened and the ground state is a doublet.

6.1. The spectral densities

As shown in section 4.2, the current is proportional to the integral of the following weighted average spectral density:

$$\rho_d^{av}(\omega) = \frac{\sum_\eta \Gamma^\eta \rho_d^\eta(\omega)}{\Gamma^s + \Gamma^t}. \tag{36}$$

However, as we will show, a study of the singlet $\rho_d^s(\omega)$ and triplet $\rho_d^t(\omega)$ parts of this average density contributes significantly to the understanding of the numerical results. As expected from section 5.4, within our numerical accuracy, the three densities, shown in figure 2, coincide with the specular

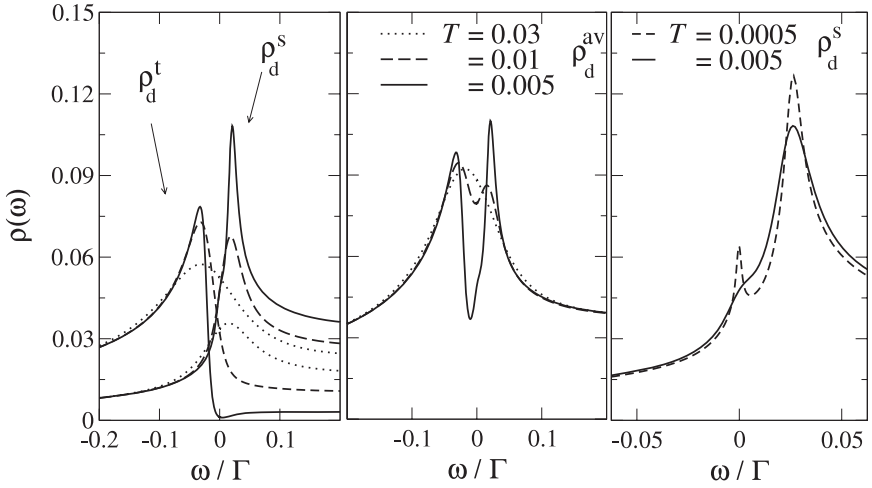

Figure 3. Spectral densities as a function of frequency for $V = 0$, $E_t = -2$, $E_s = -2.03$ and several temperatures. Left: $\rho_d^s(\omega)$ and $\rho_d^t(\omega)$, middle: weighted average (see equation (36)), right: $\rho_d^s(\omega)$ at low temperatures.

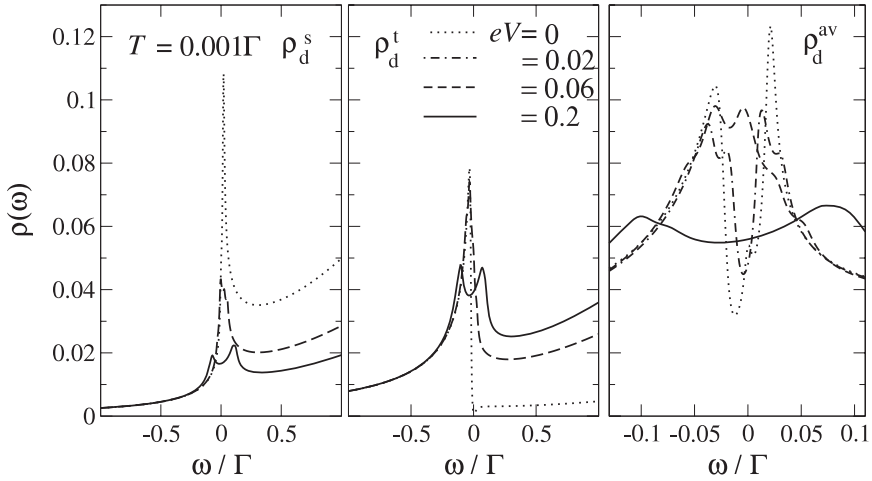

Figure 4. Spectral densities $\rho_d^s(\omega)$ and $\rho_d^t(\omega)$ as a function of frequency for $T = 0.001\Gamma$, $E_t = -2$, $E_s = -2.03$ and several bias voltages.

image of that of the OAM times a factor 1/2 (figure 5 of [51]). At equilibrium, they show a peak at the Fermi level. The width of this peak allows us to define a Kondo temperature T_K. Under an applied bias voltage, the peak splits in two near the corresponding μ_ν as in the OAM [51].

How do the spectral densities evolve as one moves from the quantum critical line? For $V = 0$, this is shown in figure 3 on the singlet side of the transition. For small temperatures, decreasing E_s from the quantum critical line ($E_t = E_s$), $\rho_d^s(\omega)$ displaces to positive frequencies, while $\rho_d^t(\omega)$ decreases and displaces its weight to negative frequencies. As a consequence, a pseudogap opens in $\rho_d^{av}(\omega)$. A similar pseudogap was found before in studies of two-level systems and interpreted as the low temperature part of a two-stage Kondo effect [40], along the lines discussed in sections 3.2 and 5.2. At very low temperatures (below 0.005Γ), a spurious spike appears at the Fermi energy in $\rho_d^s(\omega)$. This is due to a known shortcoming of the NCA that takes place when the ground state for zero hybridization is non-degenerate, for example under an applied magnetic field [51]. However, as argued in [51] it is interesting to note that this shortcoming does not affect the calculation of thermodynamic properties under a finite applied magnetic field [60].

The densities under an applied voltage are shown in figure 4. The main effect of the bias voltage V is to lead to a decrease of the singlet part of the density $\rho_d^s(\omega)$ and a simultaneous increase of the triplet part $\rho_d^t(\omega)$ for positive frequencies. In addition, near the average Fermi level $(\mu_L + \mu_R)/2$, as V is increased, the pseudogap in the average density of states $\rho_d^{av}(\omega)$ first closes, leading roughly to a single broader peak near $(\mu_L + \mu_R)/2$, and then, for larger V, this peak in $\rho_d^{av}(\omega)$ splits in two near μ_L and μ_R as in figure 2 and the ordinary Anderson model [51]. The right panel of figure 4 shows $\rho_d^{av}(\omega)$ with more detail at low energies and including another small voltage. This fine structure suggests that, as the gate voltage is applied, the peaks of $\rho_d^\eta(\omega)$ split in two, shifted $\pm eV/2$. Then, naturally, the pseudogap closes when eV reaches the difference between the position of the peaks, which is near $E_t - E_s$.

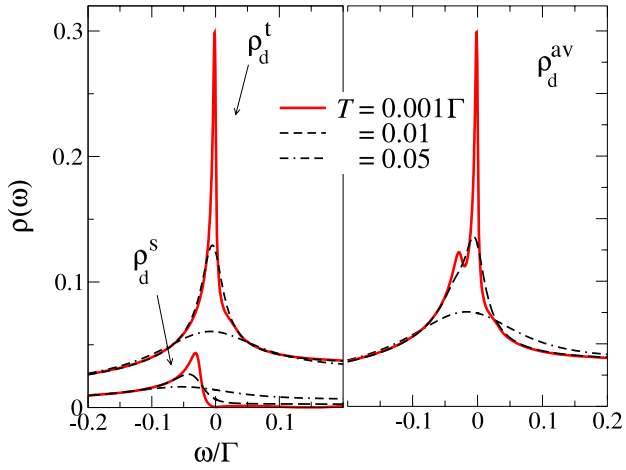

Figure 5. Spectral densities $\rho_d^s(\omega)$ and $\rho_d^t(\omega)$ as a function of frequency for $V = 0$, $E_t = -2$, $E_s = -1.97$ and several temperatures.

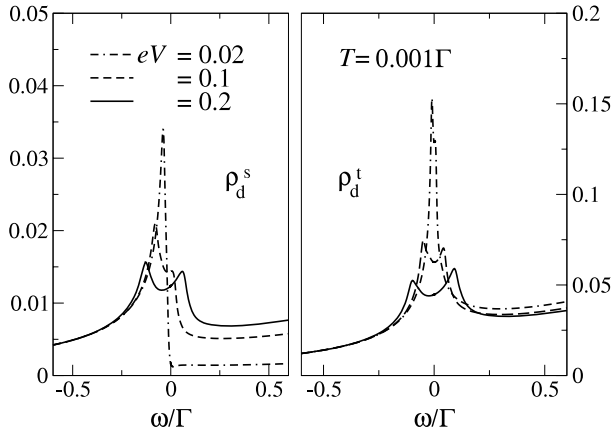

Figure 6. Spectral densities $\rho_d^s(\omega)$ and $\rho_d^t(\omega)$ as a function of frequency $T = 0.001\Gamma$, $E_t = -2$, $E_s = -1.97$ and several bias voltages.

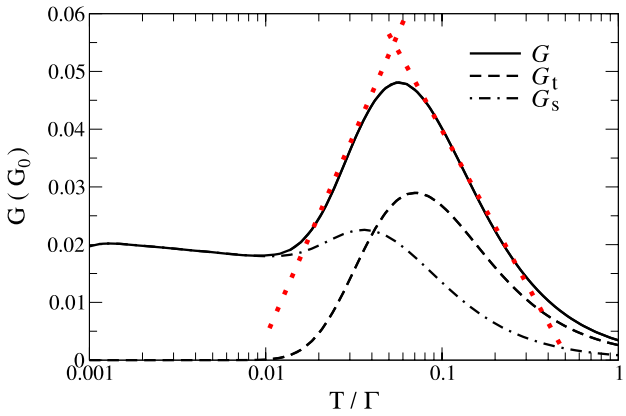

Figure 7. Zero bias conductance $G(T, 0)$ in units of $G_0 = 2e^2A/h$ as a function of temperature (full line) and contributions from the singlet (dashed–dotted line) and triplet (dashed line) for $E_t = -3$, $E_s = -3.1$. Straight dotted lines are guides to the eyes.

The spurious peak at the Fermi level disappears already for very small bias voltages.

The spectral densities on the triplet side of the transition ($E_s > E_t$) at equilibrium are shown in figure 5. In this case, the ground state for $V_s = V_t = 0$ is degenerate and no spurious peaks appear. Therefore our results are more robust. In contrast to the previous case, $\rho_d^t(\omega)$ remains peaked at the Fermi energy for low temperatures. This is a consequence of the partial Kondo effect, by which the spin 1 at the dot forms a ground state doublet with the conduction electrons of both leads, as is known from the exact solution of the model when the singlet can be neglected [2, 35, 36] or the spin-1 underscreened Kondo model [24, 25].

The singlet part of the density $\rho_d^s(\omega)$ displaces to negative frequencies in this case. Therefore a pseudogap also appears in $\rho_d^{av}(\omega)$, but at finite frequencies. Note that at high temperatures both densities are similar except for a constant factor and the difference in the structure of $\rho_d^s(\omega)$ and $\rho_d^t(\omega)$ develops at a characteristic temperature of the order of a fraction of $|E_s - E_t|$.

The effect of an applied bias voltage on these densities is shown in figure 6. In this case, the singlet part of the density increases with voltage at positive frequencies, in contrast to the case shown above (figure 4) for the singlet side of the transition. However, the behavior of $\rho_d^{av}(\omega)$ near the average Fermi energy is similar as in the above case. The peaks at equilibrium first broaden and merge into one for small bias voltage V, and for larger V this peak splits in two centered at energies near μ_L and μ_R.

6.2. The equilibrium conductance

The conductance $G(T, V) = dI/dV$ for $V = 0$ on the singlet side of the transition is shown in figure 7 together with the contributions of the singlet ($\Gamma^s \rho_d^s(\omega)$ in equation (17)) and triplet ($\Gamma^t \rho_d^t(\omega)$) part of the spectral densities. Our result agree with previous ones using NRG [31, 40] and with experiment [39]. In particular, the increase and decrease of $G(T)$ from its maximum value are logarithmic to a good degree of accuracy. At very low temperatures (below 0.01Γ in figure 7), our result for $G(T)$ increases slightly as the temperature is lowered, while one expects a saturation at a value given by the generalized Friedel–Luttinger sum rule [31] (see below). This low temperature increase is due to the spurious peak that develops in $\rho_d^s(\omega)$ as a consequence of the NCA, as explained in section 6.1.

According to the generalized Friedel–Luttinger sum rule [31], the conductance $G(T, V)$ at zero temperature and without applied bias voltage on the singlet side of the transition is given by

$$G_s(0,0) = G_0 \sin^2\left(\frac{\pi}{2} n_{\rm odd}\right), \tag{37}$$

where $G_0 = 2e^2A/h$ and $n_{\rm odd} = \langle \sum_\sigma |\sigma\rangle\langle\sigma| \rangle = 1 - \langle |00\rangle\langle 00| + \sum_M |1M\rangle\langle 1M| \rangle$ is the total occupation of the configuration with odd number of particles. For the parameters of figure 7, we obtain $n_{\rm odd} = 0.10 \approx 0$ and then one expects a low value of $G_s(00)/G_0$. In fact, inserting this value of $n_{\rm odd}$ in equation (37) one obtains $G_s(0,0)/G_0 = 0.0245$. Our corresponding result is near 0.020 (see figure 7). Although it is known that the NCA does not satisfy Fermi

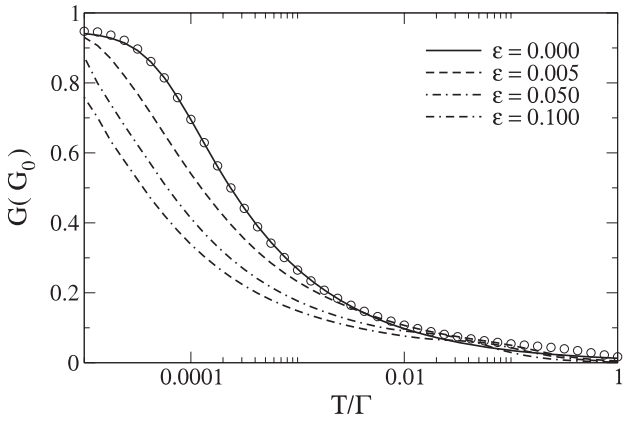

Figure 8. Zero bias conductance $G(T)$ as a function of temperature for $E_t = -3$ and several values of $\varepsilon = E_s - E_t$ (increasing from top to bottom). The circles correspond to equation (38).

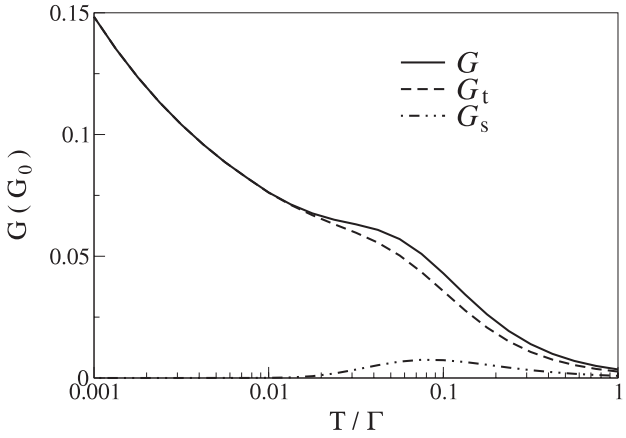

Figure 9. Zero bias conductance $G(T)$ as a function of temperature (full line) and contributions from the singlet (dashed–double-dotted line) and triplet (dashed line) for $E_t = -3$, $E_s = -2.9$.

liquid relationships, the deviation (near 0.005) is not too large for a magnitude that is, in general, of the order of 1. For the particular case of figure 7, the deviation is near 10% of the maximum value shown in the figure.

The evolution of the zero bias conductance as the system moves from the quantum critical line $E_t = E_s$ to the triplet side of the transition $E_t < E_s$ is shown in figure 8. At the transition, the conductance is the same as that of an OAM [51], with parameters given by the equivalence explained in sections 5.1 and 5.3. In particular, we find that the conductance is very well described by the empirical curve derived by fitting results of the NRG for a spin 1/2:

$$G_E(T) = \frac{G(0)}{\left[1 + (2^{1/s} - 1)(T/T_K)^2\right]^s}, \tag{38}$$

with $s = 0.22$. As E_t is lowered, removal of degeneracies in the ground state leads to a decrease in the conductance at intermediate temperatures. At zero temperature, the generalized Friedel–Luttinger sum rule [31], for the triplet side of the transition gives

$$G_t(0,0) = G_0 \cos^2\left(\frac{\pi}{2} n_{\text{odd}}\right). \tag{39}$$

Since the valence is only slightly increased by a small decrease in E_t, one expects that $G(0,0) \approx G_0$ in good agreement with our results. The temperatures reached in our NCA approach for the larger values of $\varepsilon = E_s - E_t$ used in figure 8 are not low enough to reach these high values of the conductance.

A distinct feature of $G(T,0)$ on the triplet side of the transition is the developing of a bump or a plateau at intermediate temperatures. This is more clearly displayed in figure 9 where the scale in the conductance has been expanded. This structure has not been noticed in previous NRG calculations of the conductance in two-level systems [31, 40]. This might be due to insufficient calculations in the appropriate range of temperatures (which correspond to rather small values of the conductance). Another possible reason is the loss of resolution of NRG for high energy features. This shortcoming of NRG is clearly manifest [61, 62] in systems of two QDs in which the Kondo resonance is split in two [61–63]. The separation of the spectral density $\rho_d^{\text{av}}(\omega)$ which enters the equation for the current (17) into singlet and triplet components, as shown in figure 9, shows that the bump is due to charge excitation involving the singlet component (which is peaked at an energy $E_s - E_t$, see figure 3) broadened by the temperature.

This provides an interpretation of the corresponding transport experiments through C_{60} QDs (figure 4(b) of [39]). The comparison suggests that, in general, the temperature in the experiment could not be lowered significantly after the plateau has been completed, and that the conductance should continue to increase for decreasing temperatures. Roch *et al* [39] suggested a different physical picture, fitting the plateau with the empirical equation (38) with a smaller value of G_0 and speculated that the further increase in $G(T,0)$ at smaller temperatures might be due to the opening of another parallel transport mode. The effect of a second screening is expected to lead to a decrease of the conductance on general physical grounds [29]. Our results also indicate that, while equation (38) is a good curve fitting for the conductance of the OAM, it does not work in the STAM for general values of the parameters. An exception is, of course, the exactly solvable quantum critical line in which the STAM is mapped onto an OAM plus a free spin [37], as described in section 5.

6.3. *Conductance as a function of bias voltage*

In figure 10 we show the differential conductance $G(T,V) = \mathrm{d}I/\mathrm{d}V$ as a function of bias voltage for small temperatures and for three values of $\varepsilon = E_s - E_t$. One of them ($\varepsilon = 0$) corresponds to the quantum critical transition and for the other two, the system is either on the singlet ($\varepsilon < 0$) or triplet ($\varepsilon > 0$) side of the transition. The remarkable change of behavior at the transition is evident. As expected from the results of section 6.1, the opening of a gap in $\rho_d^{\text{av}}(\omega)$ near the Fermi energy on the singlet side of the transition, leads to a dip in $G(0,V)$ at low V. The width of this dip is of the order of $|\varepsilon|$. At the bottom of the dip, the small value of the conductance

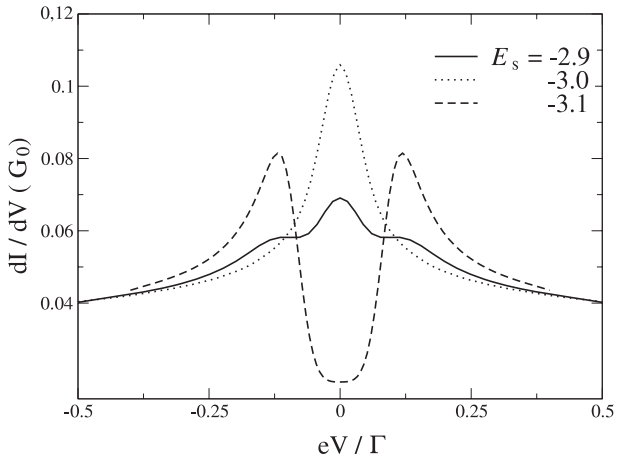

Figure 10. Differential conductance as a function of bias voltage V for $T = 0.01$, $E_t = -3$ and several values of E_s.

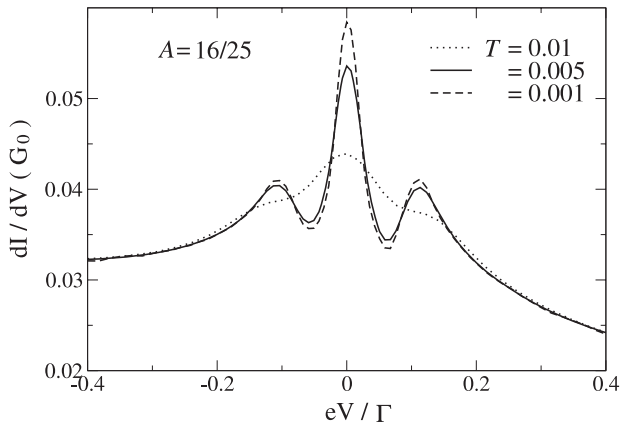

Figure 11. Differential conductance as a function of bias voltage for $E_t = -3$, $E_s = -2.9$ and several temperatures.

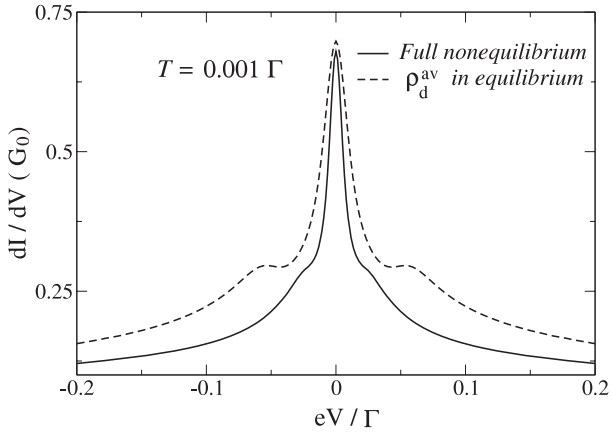

Figure 12. Full line: differential conductance as a function of bias voltage for $E_t = -2$, $E_s = -1.97$ and $T = 0.001\Gamma$. Dashed line: corresponding result taking $\rho_d^{\rm av}(\omega)$ at $V = 0$.

$G(0, 0)$ should be given by the generalized Friedel–Luttinger sum rule equation (37), while the NCA results have a deviation of nearly 20% of this value, as discussed in section 6.1. For larger values of $-\varepsilon$, the dip becomes wider, and the result is similar to the conductance observed in finite chains of an even number of Mn atoms on CuN [64].

On the triplet side of the transition, a structure with a central peak at zero bias and two lateral maxima is obtained. The three peaks are more marked at smaller temperatures, as we have shown in figure 4 of [42]. This structure also agrees qualitatively with the experimental findings in C_{60} QDs (figure 4(a) of [39]). Actually the observed structure is asymmetric, in contrast to the results shown in figure 10. This is a consequence of our assumption of a symmetric voltage drop. In fact the couplings $\Gamma_{\rm L}^{\eta}$ and $\Gamma_{\rm R}^{\eta}$ are usually very different for C_{60} molecules [65] and this leads to an asymmetric voltage drop. A reasonable assumption is that the voltage drop from one lead to the molecule is inversely proportional to the coupling to the corresponding lead [58] (see footnote 5). In our calculation, the ratio between couplings enters through the asymmetry parameter A that controls the magnitude of the current (see section 4.2 and equations (17) and (19)) and the functions (24) that enter the self-consistency equations (see section 4). A calculation for an asymmetric voltage drop is shown in figure 11. We have taken $\mu_{\rm L} = 4eV/5, \mu_{\rm R} = -eV/5$ and $\Gamma_{\rm R}^{\eta}/\Gamma_{\rm L}^{\eta} = 4$ (assumed independent of $\eta = s$ or t), keeping the same sums $\Gamma_{\rm R}^{\eta} + \Gamma_{\rm L}^{\eta}$ as before. As expected, now the height of the lateral peaks is different, with the left peak as the second most intense after the central one, in agreement with experiment. The nonmonotonic behavior of $G(0, V)$ can again be qualitatively understood from the structure of the spectral densities discussed in section 6.1. Assuming as a first approximation that $\rho_d^{\eta}(\omega)$ does not depend on voltage, it is clear from equation (17) that the conductance at zero temperature $G(0, V)$ would be proportional to the average of $\rho_d^{\rm av}(\omega)$ in a window of ω of width eV around the Fermi energy. Since $\rho_d^{\rm av}(\omega)$ is peaked at the Fermi energy (as a consequence of the peak in the triplet part $\rho_d^{t}(\omega)$), $G(0, V)$ decreases with applied bias voltage V for small V. However, when the window of width eV reaches the peak in the singlet contribution $\rho_d^{s}(\omega)$, the average of the total spectral density $\rho_d^{\rm av}(\omega)$ is expected to increase and this leads to a peak in $G(0, V)$ at finite bias voltages. This explains the result shown in figure 11 at small temperatures.

For other parameters, which would correspond to another experimental situation, in particular nearer to the transition, it might happen that $\rho_d^{s}(\omega)$ broadens as a consequence of the applied bias voltage and the structure with three peaks is absent. This is the case for the parameters of figure 12, where, instead of three peaks, we obtain two small shoulders at positive and negative voltages, as shown by the full line in figure 12. The three-peak structure is, however, the general behavior expected for a system well inside the Kondo regime when $E_s - E_t$ is larger than the width of the peaks in the spectral densities.

Due to the difficulties in the calculation of nonequilibrium properties, an approximation usually made consists in taking the density of states calculated in equilibrium, and assume that it is constant with applied bias voltage. This approach, valid for non-interacting systems has been used for example in combination with first-principles calculations, to calculate

the current through single molecules [66]. Some results for the transport through two-level systems were obtained also in this approximation [31], using a formula equivalent to equation (17), but with the average density calculated for $V = 0$.

From the result presented in section 6.1 for finite V, it is clear that this procedure is not valid in general. An example is shown by the dashed line in figure 12. When the equilibrium densities are taken instead of the nonequilibrium ones, the effects of broadening of the spectral densities caused by the applied bias voltage are missed, and as a consequence, the presence of two side peaks (although broad) is still predicted for the conductance, in contrast to the full nonequilibrium calculation. Naturally, the splitting of the Kondo resonance at higher bias voltages is also missed if frozen densities are assumed (see section 6.1 and [51]).

7. Summary and discussion

We have studied the singlet–triplet Anderson model (STAM) in which a configuration with a singlet and a triplet is mixed with another one with a doublet, via the hybridization with a conduction band. This is the simplest model that describes the conductance through a multilevel quantum dot, hybridized with two leads in an effective one-channel fashion. As found earlier in intermediate valence systems [37], the model has a quantum phase transition that separates a region with a singlet ground state from another one with a doublet ground state. This transition has been studied recently in transport measurements through C_{60} quantum dots [39]. Our results provide an explanation of the observed behavior at both sides of the transition. In particular, in the region of parameters in which the ground state is a doublet, we obtain a zero bias conductance with a plateau at intermediate temperatures, which agrees with experiment. The three-peak structure observed in the nonequilibrium conductance as a function of applied bias voltage is also explained by the model. The separation of the electronic spectral density at the dot into two parts, which correspond to excitations involving either the singlet or the triplet, leads to a more transparent understanding of the underlying physics. In particular, the above-mentioned plateau and the observed peak at finite bias voltages are due to singlet excitations.

We have also studied several limits of the model, which allow us to shed light on the expected behavior of the conductance at very low temperatures and bias voltages ($G(0, 0)$), as the integer valence limits of the STAM, and an special quantum critical line in which the model can be mapped into an ordinary Anderson model plus a free spin 1/2. For $V_t = V_s$, the latter model with additional exchange interaction H' (equation (31)) is equivalent to the STAM. An analysis of H' and the integer valence limits show that the value of $G(0, 0)$ is consistent with a generalized Friedel–Luttinger sum rule derived recently [31], and which takes into account that the system is a singular Fermi liquid when the ground state is a doublet, in a similar way as the underscreened Kondo model [25]. As is clear from equations (37) and (39) this means that an abrupt conductance change takes place at the transition [31]. Although the NCA cannot reach zero temperature, our numerical results are consistent with this result. On the quantum critical line, the conductance is smoothly connected to that of the phase with a doublet ground state.

Our NCA approach has the advantage over NRG that it can be rather easily extended to the nonequilibrium regime. When the configuration with an even number of particles is the favored one (as we have assumed here), it works very well on the quantum critical line and one expects it to be accurate enough on the 'triplet' side of the transition (where the ground state is a doublet). However, on the 'singlet' side, a spurious peak in the singlet part of the spectral density develops at very small temperatures and bias voltages, rendering our results quantitatively inaccurate for these parameters. We have found that similar difficulties arise when the configuration with an odd number of particles is favored, but now on the triplet side of the transition, including the quantum critical line. In fact, the ordinary Anderson model that comes out of the mapping described in section 5.1 now has an occupation near zero and develops a spurious peak at low temperatures and bias voltages.

While our results on the triplet side of the transition agree with the experimental results of Roch *et al* [39], and the interpretation of them is rather simple, we cannot totally rule out the possibility that some of them are due to the NCA approximation, and that the physical explanation of the observed phenomena is different. For example, the plateau of the conductance on the triplet side of the transition has not been reported in previous NRG calculations [31, 40]. We believe that this might be due to the lack of resolution of the NRG at finite frequencies [61, 62] This might be improved by averaging over different shifted logarithmic discretizations (z averaging) [67, 68] and using recent developments (the full density matrix NRG) [69, 70]. In any case, taking into account the difficulties to extend the technique out of equilibrium [71], it seems that a combination of both techniques (numerical renormalization group and non-crossing approximation) might be suitable to obtain further progress.

Acknowledgments

One of us (AAA) is supported by CONICET. This work was done in the framework of projects PIP 5254 and PIP 6016 of CONICET, and PICT 2006/483 and 33304 of the ANPCyT.

References

[1] Lawrence J M, Riseborough P S and Parks R D 1981 *Rep. Prog. Phys.* **44** 1
[2] Aligia A A, Balseiro C A and Proetto C R 1986 *Phys. Rev.* B **33** 6476 references therein
[3] Stewart G R 1984 *Rep. Prog. Phys.* **56** 755
[4] Hewson A C 1993 *The Kondo Problem to Heavy Fermions* (Cambridge: Cambridge University Press)
[5] León Hilario L M, Bruchhausen A, Lobos A M and Aligia A A 2007 *J. Phys.: Condens. Matter* **19** 176210
[6] Bruchhausen A, León Hilario L M, Aligia A A, Lobos A M, Fainstein A, Jusserand B and André R 2008 *Phys. Rev.* B **78** 125326
[7] Schrieffer J R and Wolff P A 1966 *Phys. Rev.* **149** 491

[8] Goldhaber-Gordon D, Shtrikman H, Mahalu D, Abusch-Magder D, Meirav U and Kastner M A 1998 *Nature* **391** 156
[9] Cronenwet S M, Oosterkamp T H and Kouwenhoven L P 1998 *Science* **281** 540
[10] van der Wiel W G, de Franceschi S, Fujisawa T, Elzerman J M, Tarucha S and Kowenhoven L P 2000 *Science* **289** 2105
[11] Manoharan H C, Lutz C P and Eigler D M 2000 *Nature* **403** 512
[12] Nagaoka K, Jamneala T, Grobis M and Crommie M F 2002 *Phys. Rev. Lett.* **88** 077205
[13] Knorr N, Schneider M A, Diekhöner L, Wahl P and Kern K 2002 *Phys. Rev. Lett.* **88** 096804
[14] Jamneala T, Madhavan V and Crommie M F 2001 *Phys. Rev. Lett.* **87** 256804
[15] Újsághy O, Kroha J, Szunyogh L and Zawadowski A 2000 *Phys. Rev. Lett.* **85** 2557
[16] Plihal M and Gadzuk J W 2001 *Phys. Rev.* B **63** 085404
[17] Aligia A A and Lobos A M 2005 *J. Phys.: Condens. Matter* **17** S1095 references therein
[18] Merino J and Gunnarsson O 2004 *Phys. Rev. Lett.* **93** 156601
[19] Merino J and Gunnarsson O 2004 *Phys. Rev.* B **69** 115404
[20] Lin C-Y, Castro Neto A H and Jones B A 2005 *Phys. Rev.* B **71** 035417
[21] Aligia A A 2006 *Phys. Rev. Lett.* **96** 096804
[22] Liang W, Shores M P, Bockrath M, Long J R and Park H 2002 *Nature* **417** 725
[23] Tarucha S, Austing D G, Tokura Y, van der Wiel W G and Kouwenhoven L P 2000 *Phys. Rev. Lett.* **84** 2485
[24] Sacramento P D and Schlottmann P 2007 *J. Phys.: Condens. Matter* **19** 176210
[25] Mehta P, Andrei N, Coleman P, Borda L and Zarand G 2005 *Phys. Rev.* B **72** 014430
[26] Sasaki S, De Franceschi S, Elzerman J M, van der Wiel W G, Eto M, Tarucha S and Kouwenhoven L P 2000 *Nature* **405** 764
[27] Schmid J, Weis J, Eberl K and Klitzing K V 2000 *Phys. Rev. Lett.* **84** 5824
[28] Kogan A, Granger G, Kastner M A, Goldhaber-Gordon D and Shtrikman H 2003 *Phys. Rev.* B **67** 113309
[29] Pustilnik M and Glazman L I 2001 *Phys. Rev. Lett.* **87** 216601
[30] Posazhennikova A, Bayani B and Coleman P 2007 *Phys. Rev.* B **75** 245329 references therein
[31] Logan D E, Wright C J and Galpin M R 2009 *Phys. Rev.* B **80** 125117 references therein
[32] Mazzaferro J, Balseiro C A and Alascio B 1981 *Phys. Rev. Lett.* **47** 274
[33] Aligia A A and Alascio B 1984 *J. Magn. Magn. Mater.* **43** 119
[34] Aligia A A and Alascio B 1985 *J. Magn. Magn. Mater.* **46** 321
[35] Aligia A A, Proetto C R and Balseiro C A 1985 *Phys. Rev.* B **31** 6143(R)
[36] Aligia A A, Balseiro C A, Proetto C R and Schlottmann P 1987 *J. Magn. Magn. Mater.* **63/64** 231 references therein
[37] Allub R and Aligia A A 1995 *Phys. Rev.* B **52** 7987
[38] Sachdev S 1999 *Quantum Phase Transitions* (Cambridge: Cambridge University Press)
[39] Roch N, Florens S, Bouchiat V, Wernsdorfer W and Balestro F 2008 *Nature* **453** 633
[40] Hofstetter W and Schoeller H 2001 *Phys. Rev. Lett.* **88** 016803
[41] Paaske J, Rosch A, Wölfle P, Mason N, Markus C M and Nygard J 2006 *Nat. Phys.* **2** 460
[42] Roura-Bas P and Aligia A A 2009 *Phys. Rev.* B **80** 035308
[43] Aligia A A 2006 *Phys. Rev.* B **74** 155125
[44] Roura-Bas P, Vildosola V and Llois A M 2007 *Phys. Rev.* B **75** 195129
[45] Roura-Bas P, Barral M A and Llois A M 2009 *Phys. Rev.* B **79** 075410
[46] Hofstetter W and Zarand G 2004 *Phys. Rev.* B **69** 235301
[47] Batista C and Aligia A A 1992 *Solid State Commun.* **83** 419
[48] Wilson K G 1975 *Rev. Mod. Phys.* **47** 773
[49] Vojta M, Bulla R and Hofstetter W 2002 *Phys. Rev.* B **65** 140405(R)
[50] Meir Y and Wingreen N S 1992 *Phys. Rev. Lett.* **68** 2512
[51] Wingreen N S and Meir Y 1994 *Phys. Rev.* B **49** 11040
[52] Cox D L and Ruckenstein A E 1993 *Phys. Rev. Lett.* **71** 1613
[53] Hettler M, Kroha J and Herschfield S 1998 *Phys. Rev.* B **58** 5649
[54] Bulla R, Costi T A and Pruschke T 2008 *Rev. Mod. Phys.* **80** 395 references therein
[55] Aligia A A and Proetto C R 2002 *Phys. Rev.* B **65** 165305 references therein
[56] Cornaglia P S and Grempel R D 2005 *Phys. Rev.* B **71** 075305
[57] Hewson A C, Bauer J and Oguri A 2005 *J. Phys.: Condens. Matter* **17** 5413
[58] Rincón J, Aligia A A and Hallberg K 2009 *Phys. Rev.* B **79** 121301(R)
Rincón J, Aligia A A and Hallberg K 2009 *Phys. Rev.* B **80** 079902(E)
[59] Martin-Rodero A, Levy Yeyati A, Flores F and Monreal R C 2008 *Phys. Rev.* B **78** 235112
[60] Bauer E D, Wang C, Fanelli V R, Lawrence J M, Goremychkin E A, de Souza N R, Ronning F, Thompson J D, Silhanek A V, Vildosola V, Lobos A M, Aligia A A, Bobev S and Sarrao J L 2008 *Phys. Rev.* B **78** 115120
[61] Vaugier L, Aligia A A and Lobos A M 2007 *Phys. Rev. Lett.* **99** 209701
[62] Vaugier L, Aligia A A and Lobos A M 2007 *Phys. Rev.* B **76** 165112
[63] Dias da Silva L G G V, Sandler N P, Ingersent K and Ulloa S E 2006 *Phys. Rev. Lett.* **97** 096603
[64] Hirjibehedin C F, Lutz C P and Heinrich A J 2006 *Science* **312** 1021
[65] Scott G D, Keane Z K, Ciscek J W, Tour J M and Natelson D 2009 *Phys. Rev.* B **79** 165413
[66] Heurich J, Cuevas J C, Wenzel W and Schön G 2002 *Phys. Rev. Lett.* **88** 256803
[67] Yoshida M, Whitaker M A and Oliveira L N 1990 *Phys. Rev.* B **41** 9403
[68] Žitko R and Pruschke T 2009 *Phys. Rev.* B **79** 085106
[69] Peters R, Pruschke T and Anders F B 2006 *Phys. Rev.* B **74** 245114
[70] Weichselbaum A and von Delft J 2007 *Phys. Rev. Lett.* **99** 076402
[71] Anders F B 2008 *Phys. Rev. Lett.* **101** 066804